AIAA JOURNAL
Vol. 45, No. 8, August 2007

Implicit High-Order Time-Marching Schemes for the Linearized Euler Equations

George Arambatzis,* Panagiotis Vavilis,* Ioannis Toulopoulos,† and John A. Ekaterinaris‡
Foundation for Research and Technology—Hellas, 711 10 Heraklion, Crete, Greece

DOI: 10.2514/1.25336

High-order-accurate implicit time-marching methods are presented for discontinuous Galerkin and spectral volume high-order-accurate spatial discretizations of the linearized Euler equations that govern propagation of aeroacoustic disturbances. It is found that despite the additional computational time that is required for the solution of the large, sparse linear system for the degrees of freedom of high-order spectral volume or discontinuous Galerkin discretizations, implicit methods offer an attractive alternative for practical aeroacoustic computations with these high-order methods. Several explicit and implicit methods for time advancement are tested. The advantages of implicit higher-order-accurate (in time) methods that involve multiple implicit steps are demonstrated. The efficiency and accuracy of time-marching methods is evaluated for test problems with exact solutions. It is shown that complex domain aeroacoustic predictions can be obtained at a reduced computational cost with the use of high-order-accurate implicit methods.

I. Introduction

EXPLICIT methods for time marching of discontinuous Galerkin (DG) space discretizations of the linearized and nonlinear Euler equations have been introduced by Cockburn and Shu [1]. The same explicit methods were used for time-marching spectral volume (SV) discretizations introduced by Wang et al. in a series of papers [2–5]. The advantages of these matrix-free explicit methods are high order of accuracy in time, simplicity in implementation, and low computational cost per time step. These methods were recently used for aeroacoustic computations with the DG method of simple and moderate-sized aeroacoustic problems [6]. However, explicit methods are subjected to severe Courant–Friedrichs–Lewy (CFL) stability limitations.

Atkins and Shu [7] demonstrated that the increase of the order of accuracy of the DG space discretizations or the degree of the polynomials that are used for the expansion in the local finite element space rapidly lowers the CFL number and causes increasingly more stringent time-step limitations. Analogous limitations are encountered with the SV method [2]. The CFL stability for high-order SV or DG discretizations is significantly lower than the CFL stability of equivalent-order finite difference or finite volume high-order methods [8,9]. As a result, the computational effort of explicit methods for time-accurate solutions of problems that require unstructured meshes with high-order DG or SV discretizations is so high that the overall numerical scheme often becomes inefficient. Indeed, in [6] it was concluded that the computational time for DG discretizations of an order higher than four is rather excessive for explicit time-marching algorithms. Therefore, the efficient application of high-order implicit time-marching methods for time-accurate computations is investigated in this paper.

Recently, several investigators attempted to circumvent the severe time-step limitations of DG discretizations using implicit time-marching methods [10–13] and multigrid acceleration [14–17]. Furthermore, the ADER scheme [18,19], or space–time finite elements [20,21], may be used for higher-order-accurate time marching of conservation laws discretized in space with the discontinuous Galerkin method. In addition, high-order-accurate implicit time-marching schemes were developed for the numerical solution of linear [22,23] and nonlinear [24–27] conservation laws and applied in the finite difference or the finite volume context.

The objective of this work is to demonstrate the efficiency and accuracy of high-order-accurate implicit schemes for time advancement of the linearized Euler equations discretized in space with the finite element framework of the SV or the DG high-order methods. Successful application of these schemes to aeroacoustics is expected to have an impact in other areas of computational sciences such as unsteady aerodynamics, computational electromagnetics, and magnetogasdynamics, in which high-order-accurate time marching is required, and it was proven that high-order-accurate DG discretizations yield superior performance compared with other spatial discretization methods [28]. Extension of the high-order implicit methods to the nonlinear Euler and Navier–Stokes equations for nonlinear acoustic propagation and large eddy simulations. is also possible.

It is well known that application of implicit methods significantly increases the memory requirements. The main advantage of implicit methods for DG and SV high-order-accurate (in space) discretizations is that they can advance the solution with significantly larger time steps than with the explicit methods, for both steady-state [10] and time-accurate solutions [11]. The high CFL numbers achieved with implicit methods are necessary for the efficient numerical solution of viscous flow problems in complex geometries. However, for numerous aeroacoustic applications, the use of implicit time integration is solemnly needed. The increase of the allowable time step for linear and nonlinear conservation laws is obtained at the expense of an increased computational cost per time step that results from the solution of a large system of linear equations.

For DG and SV discretizations, the approximate solution is considered discontinuous at the element interfaces and a numerical flux is introduced to provide the communication between adjacent elements. As a result, implicit schemes with DG and SV methods require additional computational time for the calculation of the residual Jacobians for the products of both physical and numerical fluxes and the test functions [10]. The large amount of memory that is

Presented as Paper 3548 at the 36th AIAA Fluid Dynamics Conference and Exhibit, San Francisco, CA, 5–8 June 2006; received 20 May 2006; revision received 23 January 2007; accepted for publication 5 April 2007.

*Institute of Applied and Computational Mathematics, P.O. Box 1385; currently Graduate Student, School of Mechanical and Aerospace Engineering, University of Patras, Patras, Greece.

†Institute of Applied and Computational Mathematics, P.O. Box 1385; currently Graduate Student, School of Mathematics, University of Athens, Athens, Greece.

‡Institute of Applied and Computational Mathematics, P.O. Box 1385; currently Professor, School of Mechanical and Aerospace Engineering, University of Patras, Patras, Greece. Associate Fellow AIAA.

necessary for the storage of the flux Jacobians and the large matrix of the linear system [even with sparse-storage generalized minimal residual (GMRES) algorithms], is another problem encountered with implicit solvers for the DG and SV methods. For large-sized meshes, the memory required for GMRES can outnumber the memory of usual desktops. Therefore, for large-sized problems and three-dimensional applications, the use of domain decomposition techniques would be necessary with implicit methods.

In this paper, we demonstrate the effectiveness of classical implicit schemes and a fourth-order-accurate implicit method [24] for time advancement of the linearized Euler equations. Other high-order implicit time-marching methods [22,23], developed for finite difference discretizations, could also be considered in the DG finite element framework. Furthermore, classical explicit Runge–Kutta (RK) methods and standard implicit methods are also compared and evaluated.

II. Governing Equations

The linearized Euler equations governing propagation of isentropic acoustic disturbances are

$$\frac{\partial q}{\partial t} + [A]\frac{\partial q}{\partial x} + [B]\frac{\partial q}{\partial y} = S \tag{1}$$

where q is the solution variable vector and $[A]$ and $[B]$ are constant matrices given by

$$q = \begin{bmatrix} u \\ v \\ p \end{bmatrix}, \qquad A = \begin{bmatrix} U & 0 & 1 \\ 0 & U & 0 \\ 1 & 0 & U \end{bmatrix}, \qquad B = \begin{bmatrix} V & 0 & 0 \\ 0 & V & 1 \\ 0 & 1 & V \end{bmatrix} \tag{2}$$

Note that in contrast to the full Euler equations, in the linearized Euler equations, the matrices $[A]$ and $[B]$ are constant.

III. Space Discretization

The SV and DG methods were used for high-order-accurate discretizations in space. The main advantage of these methods is that they achieve high-order accuracy for unstructured meshes using high-order polynomial expansion of the approximate solution within the element and they do not require large-sized stencils. In addition, they are suitable for shock capturing. Both the SV and the DG methods were successfully applied for triangular or tetrahedral unstructured grids, and it was found that the accuracy of the numerical solution does not depend strongly on the smoothness of the mesh. It was demonstrated, however, that with the increase of the order of the spatial approximation the CFL stability, both methods degrade considerably. For example, the theoretical CFL of the explicit RK3 method for finite differences (see [29]) is 1.73, whereas for DG discretizations (see [7]) it is 0.13 and 0.066 for P^3 and P^5 polynomial expansions, respectively. As a result, long time integration with explicit time-marching methods and DG or SV spatial discretization of an order higher than second (P^1 polynomial expansions) becomes very intensive computationally and impractical for many industrial applications that require computation of unsteady viscous flows and acoustic wave propagation in complex domains.

On the other hand, application of more stable implicit time-marching schemes for high-order-accuracy (in space) SV and DG discretizations of the full Euler equations requires evaluation of Jacobian matrices for each time step and computationally intensive inversion of large matrices. For the linearized Euler equations, evaluation of the residual Jacobian is not required, implicit methods are unconditionally stable, and the time-step limitations may occur only from application of boundary conditions. Therefore, implicit time marching with large time steps, despite the added cost of large matrix inversion, could potentially offer an attractive alternative to explicit time marching, especially for long time integration in complex domains, which inevitably include small elements. It is emphasized that for time-accurate calculations, similarly to explicit methods [29], the time-step size of implicit methods is still bounded by accuracy requirements. To better demonstrate the implicit time-integration schemes for DG and SV, spatial discretizations of the linearized Euler equations for the SV and DG methods are outlined next.

A. Spectral Volume Method

The basic idea of the spectral volume method is presented for the following one-dimensional conservation law for the scalar $u(x, t)$,

$$\frac{\partial}{\partial t}u(x,t) + \frac{\partial}{\partial x}f[u(x,t)] = 0 \tag{3}$$

in the domain Ω, with initial condition $u(x, 0) = u_0(x)$ and appropriate boundary conditions.

The domain Ω is discretized into N nonoverlapping cells S_i, called spectral volumes, which are the same as the usual finite volumes. Given a desired spatial order of accuracy k, each spectral volume S_i is subdivided into k control volumes (CVs). The jth CV of S_i, denoted by $C_{i,j}$, is

$$C_{i,j} = (x_{i,j-1/2}, x_{i,j+1/2}), \qquad j = 1, \ldots, k \tag{4}$$

The performance of the SV methods depends on the subdivision of the SV into CVs.

The cell-averaged state variable at time t for the control volume $C_{i,j}$ is defined as

$$\bar{u}_{i,j}(t) = \frac{1}{h_{i,j}}\int_{C_{i,j}} u(x,t)\,\mathrm{d}x \tag{5}$$

where $h_{i,j} = x_{i,j+1/2} - x_{i,j-1/2}$.

Using these definitions, the reconstruction problem in the SV method is as follows. Given the cell-averaged state variables $\bar{u}_{i,j}$ for all the CVs in S_i, construct a polynomial $p_i(x)$ of degree $k-1$ at most, such that $p_i(x)$ is the kth-order approximation to the function $u(x)$, inside S_i. The solution at the CV interfaces must be computed to update the solution at the next time level. The solution at the CV interfaces is expanded through a set of basis functions $\{\varphi_l\}_{l=1}^{k}$ as follows:

$$u_{i,j+1/2} = \sum_{l=1}^{k} \bar{u}_{i,l}\varphi_l(x_{j+1/2}) \tag{6}$$

For linear problems, the order of accuracy of this expansion is $k+1$.

The appropriate basis set is defined by following the procedure described in [2] to obtain the values of the basis functions on the CV interfaces:

$$c_{j,l} = \varphi_l(x_{i,j+1/2}) = h_{i,l}\sum_{r=l}^{k}\frac{1}{\omega'(x_{i,r+1/2})}\sum_{\substack{m=0\\ m\neq r}}^{k}\prod_{\substack{q=0\\ q\neq r,m}}^{k}(x_{i,j+1/2} - x_{i,j-1/2}) \tag{7}$$

where ω' is the derivative of

$$\omega(x) = \sum_{j=0}^{k}(x - x_{i,j+1/2})$$

Finally, we can write the conservation law (3) in the semidiscrete form:

$$\frac{\mathrm{d}}{\mathrm{d}t}\bar{u}_{i,j} + \frac{1}{h_{i,j}}\left(\hat{f}_{i,j+1/2} - \hat{f}_{i,j-1/2}\right) = 0 \tag{8}$$

where $\hat{f}_{i,j+1/2}$ is a numerical flux. At the CV interfaces, the solution is continuous, therefore $\hat{f}_{i,j+1/2} = f(x_{i,j+1/2})$. However, on the SV interfaces, the solution may be discontinuous. Therefore, the numerical fluxes at $x_{i\pm1/2}$ are computed with a Riemann solver or a

flux-splitting technique. The SV method idea described in one dimension was extended for systems of conservation laws and multidimensional applications. It was also shown that the SV method is basically a Galerkin method [30]. The main difficulty with the extension of the SV method to multidimensions is subdivision of the spectral volumes S_i in CVs $C_{i,j}$ for triangular or tetrahedral elements for high-order expansions [4,5].

B. Discontinuous Galerkin Method

Assuming that the approximate solution q_h of the governing equations in conservation law form, $\partial_t \mathbf{q} + \nabla \cdot \mathbf{F}(\mathbf{q}) = 0$, is sought in the finite element space V_h,

$$V_h = \{u_h \in \mathbf{L}^\infty(D) : u_h|_K \in \mathbf{V}(\mathbf{K}), \forall \mathbf{K} \in T_h\} \tag{9}$$

where T_h is a discretization of the domain D using triangular or polyhedral elements, and $\mathbf{V}(\mathbf{K})$ is the local space that contains the collection of polynomials up to degree k. The weak formulation of the governing equation is

$$\frac{\mathrm{d}}{\mathrm{d}t}\int_K \mathbf{q} v(x)\,\mathrm{d}V + \sum_{e\in\partial K}\int_e \mathbf{F}(\mathbf{q})\cdot \boldsymbol{n}_{e,K} v(x)\,\mathrm{d}S - \int_K \mathbf{F}(\mathbf{q})\cdot\nabla[v(x)]\,\mathrm{d}V = 0 \tag{10}$$

where $v(x) \in \mathbf{V}(\mathbf{K})$ is any sufficiently smooth function, and $\boldsymbol{n}_{e,K}$ denotes the outward unit normal to the face or edge e of an element K.

By replacing $\mathbf{q}$ in each element K_i with its approximation $q_i^h \in V_h$, which is a polynomial expansion,

$$q_i^h = \sum_{j=1}^{d} [c_i(t)]_j P_j^k$$

for the degrees of freedom $[c_i(t)]_j$, we obtain the following semidiscrete form of the conservation law:

$$\frac{\mathrm{d}}{\mathrm{d}t}\mathbf{M}\mathbf{c} - \mathbf{S}\mathbf{c} + \sum_{e\in\partial K}\mathbf{F}_\mathbf{e}\mathbf{c} = 0 \tag{11}$$

In this equation, $\mathbf{c}$ denotes the vector of the coefficients in the polynomial expansion of the approximate solution or the degrees of freedom to be evolved in time, $\mathbf{M}$ is the mass matrix, $\mathbf{S}$ is the matrix resulting from numerical integration of the volume integrals, and $\mathbf{F}_\mathbf{e}$ is the matrix of the line integrals. For the linear problem, the spatial discretization with a kth-deg polynomial expansion, $P_j^k\ j = 1, \ldots, d$ [where, for triangular elements, $d = (k+1)(k+2)/2$], is $k+1$ order accurate. The matrices $\mathbf{M}$ and $\mathbf{S}$ are computed using appropriate quadrature rules. The line integrals are also computed using high-order quadrature rules.

For the expansion of the approximate solution, a nodal base was used for both one- and two-dimensional spacial approximations. The solution is assumed continuous within the element and discontinuous at the element boundaries. Therefore, the value of the numerical flux can be computed using any consistent, conservative exact, or approximate Riemann solver. In this work, the Lax–Friedrichs numerical flux was used.

IV. Time Discretization

The semidiscrete form for both the SV, Eq. (8), and the DG, Eq. (11), methods is

$$\frac{\mathrm{d}}{\mathrm{d}t}U + F(U) = 0 \tag{12}$$

Time discretization of Eq. (12) is performed using methods for systems of ordinary differential equations (ODEs). Application of explicit schemes for time advancement of the semidiscrete form of Eq. (12) is straightforward. However, the use of multistage explicit schemes with higher-order spatial approximations is still costly. The CFL stability of explicit schemes with DG space discretization deteriorates with the increase of the polynomial order. For example, Atkins and Shu [7] found that all first-order explicit methods for DG space discretizations are unstable for polynomials larger than P^1, whereas the CFL stability limit of the explicit RK3 method deteriorates as $\mathrm{CFL}(P^n) = 1.256, 0.409, 0.209, 0.130, 0.089$, and 0.066, with the increase of the polynomial order from $n = 0, \ldots, 5$. Implicit schemes have additional cost compared with explicit methods, because they require inversion of large-sized matrices. It will be shown, however, that the additional cost per time step of implicit schemes is still acceptable for aeroacoustic computations with meshes in which the use of small size elements is inevitable. The time-step size of both explicit and implicit time-marching methods is bounded by time-accuracy requirements [29]. However, it was found that the acceptable error level of the implicit CFL is still at least two orders of magnitude larger than the CFL limited time step of explicit methods.

Implicit time marching of linear systems of conservation laws, such as the linearized Euler equations of Eq. (12), which have been discretized in space with the SV or the DG method, implies inversion of a large matrix. The overall structure of this matrix is sparse, because each row includes a block matrix on the diagonal and off-diagonal blocks, resulting from the evaluation of the numerical flux with the adjacent elements. The size of the diagonal and off-diagonal block matrices depends on the order of accuracy of the spatial discretization. For example, in two-dimensional domains discretized with triangular elements and P^1 polynomial expansions, the size of the block matrices for the system of three equations of Eq. (1) is 9×9. The block size rapidly increases with the order k as $(k+1)(k+2)/2$; for a P^3 expansion, the block size is 30×30, and for a P^5 expansion it becomes 63×63. Inversion of the sparse matrix can be achieved either with direct methods or with GMRES. A sparse-storage form must be used for both direct methods or GMRES, because storage of the full matrix is prohibitive even for small-sized domains. The use of direct methods, which is advantageous for linear problems because the inverse may be stored, is limited to relatively smaller domains because they require more memory than the less straightforward to apply GMRES method. For large-sized problems or for three-dimensional applications, domain decomposition techniques must be used for both direct methods and GMRES.

A direct solver and the GMRES solver[§] provided by Saad [31] were used to invert the large, sparse matrix of implicit schemes. The convergence of the GMRES solver with the particular preconditioner used was assessed through direct comparison with the direct solver results. For all tests presented in the Results section, the incomplete lower/upper-with-threshold (ILUT) preconditioner was used. In addition, the performance of the incomplete lower/upper (ILU) preconditioner (without threshold) [31] and the modified ILU (MILU) preconditioner [31] was also tested. It was concluded that the ILUT preconditioner provides more flexibility because it allows the adjustment of two user-independent parameters p and τ that help to reduce memory usage and computational cost, respectively [31]. The optimal value of these parameters depends on the numbering that the grid generator assigns to the mesh, which in turn determines the sparsity pattern of the matrix. In the present study, we did not use mesh reordering schemes that could yield more favorable matrix sparsity patterns. It was found, however, that the selection of the parameters $p \approx 15 - 20$ and $\tau \approx 10^{-3} - 10^{-4}$ made possible convergence of the GMRES with two to three iterations. The criterion for the termination of GMRES was the absolute tolerance. The convergence was assessed through comparison with results obtained with the direct solver and comparisons with available exact solutions [32,33] for test problems.

Explicit methods such as the total variation diminishing (TVD)-RK3 and the classical RK4 method were used for comparison purposes. The performance of the following implicit time-marching methods is tested.

[§]Data available online at http://www-users.cs.umn.edu/~saad/software/SPARSKIT/sparskit.html [retrieved 31 May 2007].

A. Implicit Second-Order-Accurate Midpoint Rule

The second-order-accurate (in time) implicit midpoint-rule method for Eq. (12) is

$$\frac{U^{n+1}-U^n}{\mathrm{d}t}=F\left(\frac{U^{n+1}+U^n}{2}\right) \tag{13}$$

which is implemented by introducing a new variable $Z=(U^{n+1}+U^n)/2$ that satisfies

$$Z-U^n=\frac{\mathrm{d}t}{2}F(Z) \tag{14}$$

and the solution at the new time level $n+1$ is obtained by

$$U^{n+1}=2Z-U^n \tag{15}$$

B. Three-Stage, Fourth-Order-Accurate Implicit Method

The fourth-order-accurate (in time), three-stage, implicit time-advancement scheme of [24] for Eq. (12) is as follows:

$$\begin{aligned}
Z_1-U^n&=\frac{\beta_1\tau}{2}F(Z_1), \qquad \beta_1=1.3512, \qquad Y_1=2Z_1-U^n\\
Z_2-Y_1&=\frac{\beta_2\tau}{2}F(Z_2), \qquad \beta_2=-1.7024, \qquad Y_2=2Z_2-Y_1\\
Z_3-Y_2&=\frac{\beta_3\tau}{2}F(Z_3), \qquad \beta_3=1.3512, \qquad U^{n+1}=Y_3=2Z_3-Y_2
\end{aligned} \tag{16}$$

This scheme is a linear combination of three midpoint rules but achieves higher-order accuracy in time. It was developed and applied [24] for scalar conservation laws discretized with finite differences. It was found that in certain cases and for high-order discretizations, the backward step of the second stage generates matrices that are close to becoming ill-conditioned and difficult to invert. Further investigation of the properties of this scheme and extension to nonlinear conservation laws is needed.

C. Implicit RK2 Method

The implicit RK2 scheme of [11] for Eq. (12) is

$$\begin{aligned}
\left(1+\alpha\Delta t\frac{\partial F(U^n)}{\partial U}\right)K_1&=-F(U^n)\\
\left(1+\alpha\Delta t\frac{\partial F(U^n)}{\partial U}\right)K_2&=-F(U^n+\beta K_1)\\
U^{n+1}&=U^n+Y_1K_1+Y_2K_2
\end{aligned} \tag{17}$$

The values of the constants Y_1, Y_2, α, and β corresponding to an optimal second-order-accurate scheme are

$$\alpha=\frac{2-\sqrt{2}}{2}, \qquad \beta=8\alpha\left(\frac{1}{2}-\alpha\right), \qquad Y_1=1-\frac{1}{8\alpha}, \qquad Y_2=1-Y_1 \tag{18}$$

D. Implicit RK3 Method

The general form of a Runge–Kutta method for Eq. (12) is

$$\begin{aligned}
K_1&=F(t^{n,1},U^n+\mathrm{d}t\lambda K_1)\\
K_2&=F(t^{n,2},U^n+\mathrm{d}t(1-\lambda)K_1+\lambda K_2)\\
U^{n+1}&=U^n+\frac{\mathrm{d}t}{2}(K_1+K_2)
\end{aligned} \tag{19}$$

where $t^{n,1}=t^n+\lambda\,\mathrm{d}t$, $t^{n,2}=t^n+(1-\lambda)\,\mathrm{d}t$, and $\lambda=\frac{1}{2}\pm(\sqrt{3}/6)$. Clearly, the implicit schemes of Eqs. (14) and (16–19) involve one or more matrix inversions.

E. Stability

The CFL stability limit of explicit time-marching methods for DG spatial discretizations was found lower than finite difference or finite volume discretizations of equivalent accuracy [7]. For example, Fourier stability analysis of the DG method with P^0 polynomial bases and Euler explicit time integration yields the amplification factor

$$|G|=\sqrt{(1+r\cos\beta-r)^2+(r\sin\beta)^2}$$

where $r=\mathrm{CFL}=\Delta t/\Delta x$ and $\beta=\omega_m\Delta x$. As a result (see Fig. 1), time marching with the first-order-accurate Euler explicit method can be obtained with $\mathrm{CFL}_{\mathrm{DG}}=1$. The CFL stability limit for higher-order DG discretizations deteriorates, and the Euler explicit method becomes unconditionally unstable for P^2 expansions.

Fourier stability analysis of the first-order DG spatial discretizations (P^0 polynomials) advanced with the implicit second-order (in time) midpoint rule yields the amplification factor

$$|G|=\sqrt{\frac{2+(1-\cos\beta)(2r+r^2)}{2-(1-\cos\beta)(2r+r^2)}}$$

The polar plot of this equation (see Fig. 2) shows that time integration of the first-order DG spatial discretization with the midpoint rule is unconditionally stable for very large CFL.

The analysis for higher-order discretizations becomes more cumbersome. The amplification factor for the second-order DG method (P^1 polynomials) with the midpoint rule was found:

$$|G_{1,2}|=\frac{|4+6r^2(e^{-i\beta}-1)\pm 4r\sqrt{(e^{-i\beta})^2+10(e^{-i\beta})-2}|}{2\sqrt{(3r^2(\cos\beta-1)-2r(\cos\beta+2)-2)^2+(3r^2-2r)^2\sin^2\beta}}$$

The polar plot of Fig. 3 for the first and second modes, respectively, shows that the magnitude of $G_{1,2}$ is less than one for very large CFL and this method is again unconditionally stable. It is, however,

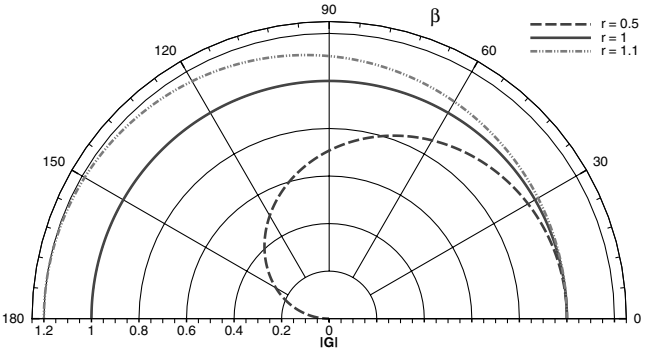

Fig. 1 Variation for the amplification factor module for the explicit Euler method.

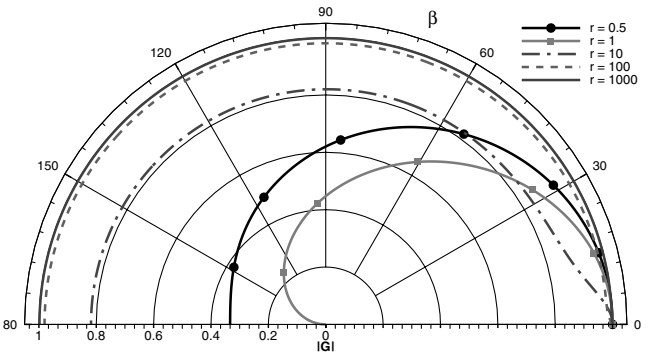

Fig. 2 Variation for the amplification factor module for the implicit midpoint 2 method with P^0.

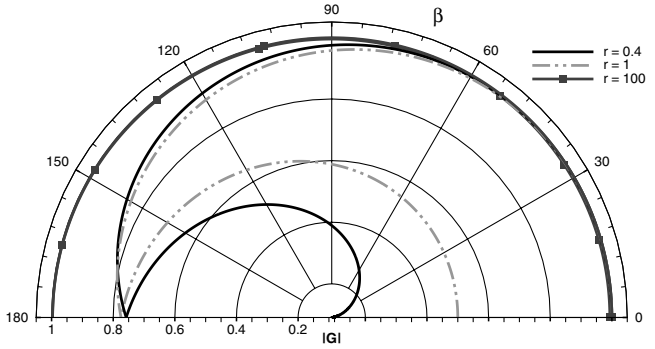

Fig. 3 Variation for the amplification factor module for the implicit midpoint 2 method with P^1.

evident that the increase of the polynomial order (see Fig. 3 in comparison with Fig. 2) causes the amplification factor for the higher-order mode to approach the unit circle for a wider range of the parameter β, even at lower CFL numbers. The multistage implicit methods are linear combinations of simple implicit schemes that, at least for low-order DG discretizations, were found to be unconditionally stable. Therefore, these schemes are expected to preserve unconditional stability.

A more detailed stability analysis of all implicit methods described in Secs. IV.A–IV.D will be presented in a separate study. It was found, however, that all implicit methods for problems that include realistic boundary conditions and high-order DG discretizations (up to sixth order in space) yielded stable time integration for large CFL numbers. The implicit CFL were at least two to three orders of magnitude larger than the CFL required for stability of explicit methods. For most test problems with uniform meshes used in this study, very large CFL numbers allowed by implicit methods cannot be used because of accuracy considerations. It is shown, however, that for more complex aeroacoustic problems such as scattering from a cylinder, shown at the end of the results section, in which small elements near the body surface are required, the use of implicit methods offers a distinct advantage over explicit methods.

V. Results

The accuracy and efficiency of spatial and temporal discretizations with different time-marching schemes and SV or DG space discretization is first demonstrated for one-dimensional convection. Numerical solutions are computed for the simple advection equation with periodic boundary conditions. First, grid convergence of the SV and DG spatial discretizations of different order of accuracy is shown in Fig. 4. A very small time step was used to make time-integration errors insignificant. The spatial accuracy in Fig. 4 was measured with the L_2 norm of the computed solution from the exact result. However, analogous grid convergence was found with other norms, such as the maximum norm. It can be seen that the design order of accuracy was achieved by both the SV and DG space discretizations, up to a very high order of spatial accuracy. The computational cost of the SV and DG methods versus error is shown in Fig. 5. It can be seen that the relative cost of both methods for a preset level of accuracy is comparable. Therefore, for two-dimensional space discretizations, we used the DG method because it appears to be more efficient, its implementation is based on the well-developed finite element framework, which is easy to extend in three dimensions, and it is more straightforward to apply than the SV method, which requires the use of complex subdivisions [5].

The convergence in time of several explicit and implicit time-marching schemes for one-dimensional convection is examined next. Time convergence in Fig. 6 was obtained using a sixth-order accurate (in space) discretization and very small grid spacing, which makes spatial errors much smaller than the error in time. It is worth mentioning that in Fig. 6, the solution for all implicit schemes was computed with the same small grid spacing, and because the time step of implicit schemes was limited only by accuracy requirements, only the time step changed. For the explicit schemes, however, a time step close to the CFL stability limit was used and the grid spacing was increased accordingly. However, for a discretization with kth-order polynomials and an nth-order-accurate (in time) scheme, the grid spacing Δx was smaller than $\Delta t^{(n/k+1)}$ to keep the spatial errors at a low level. It is evident from Fig. 6 that the implicit time-marching schemes could perform accurate time advancement with much larger CFL (the maximum CFL of all implicit schemes of Fig. 6 is approximately 25) than with explicit methods. Note, however, that the stability of implicit schemes was maintained even for CFL = 1000. In Fig. 6, only the L_2 norm of the error is shown, however, the same slope was found for other norms as well.

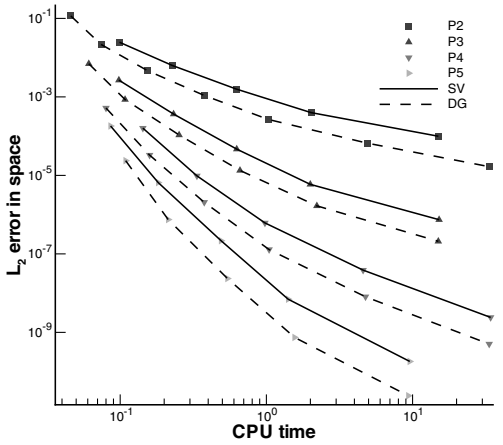

Fig. 5 Computational cost for the SV and the DG methods.

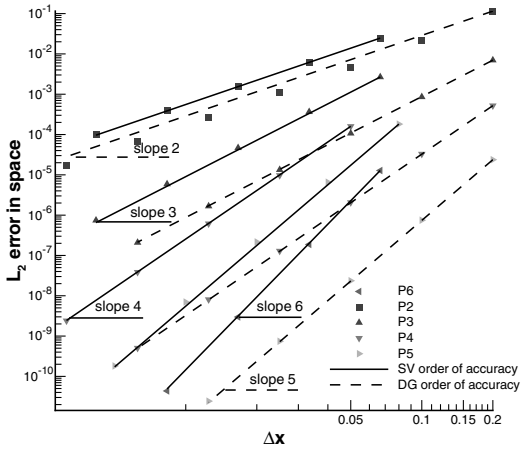

Fig. 4 Grid convergence for the SV and the DG methods.

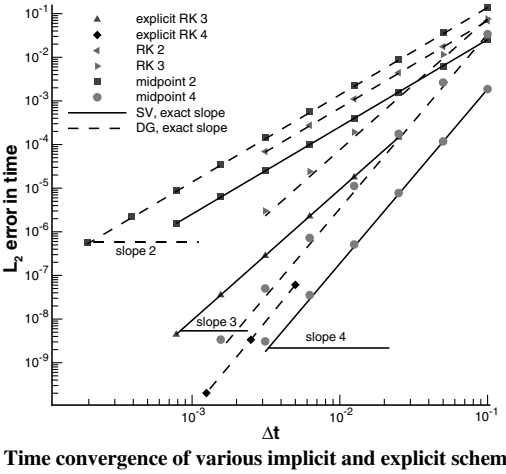

Fig. 6 Time convergence of various implicit and explicit schemes with SV and DG space discretizations.

Moreover, the convergence was examined with respect to an "exact" numerical solution that was computed with fifth-order polynomial basis, small element size, and small time step. Comparison with this "exact solution" yielded the same convergence rate.

The computational cost of various implicit time-marching schemes is shown in Fig. 7. It can be seen that for a preset high level of accuracy, the higher-order schemes offer a distinct advantage in terms of savings in computational time. Clearly, the implicit three-stage scheme of Eq. (16) is more efficient in terms of temporal error reduction than the implicit RK3 method of Eq. (19), because both methods include three stages but time marching with Eq. (16) is more accurate. In this figure, a representative computing cost of explicit methods at maximum CFL is also known.

Further demonstration of the advantages offered by implicit schemes is carried out for two-dimensional applications in simple and more complex domains. Space discretization in two dimensions is performed with the DG method that uses nodal bases and the Lax–Friedrichs numerical flux. It was verified that grid convergence of spatial discretizations is obtained for both P^1 and P^3 polynomial expansions. The time convergence of the second- and fourth-order implicit schemes of Eqs. (14) and (16), respectively, with P^3 space discretization is shown in Fig. 8. The error of the computed solutions in Fig. 8 is obtained by comparing with the analytic result. For this time convergence test, a canonical mesh with orthogonal triangles and $\Delta x = 0.01$ was used. Similar to the one-dimensional case, the convergence in time was also examined by comparing with an "exact numerical solution," which was computed with a time step $\Delta t = 10^{-6}$. It was found that both the error level and the convergence rate were the same as the rate found by comparing with the exact solution. For example, the error between the computed and the exact solution was 2.1×10^{-6}, whereas the error between the computed and the "numerical exact solution" was 2.2×10^{-6}. The convergence of the explicit schemes was performed at a constant CFL close to the stability limit and variable grid spacing.

It can be seen that for the implicit schemes of Eqs. (14) and (16) with sufficiently small time steps, the desired order of accuracy is achieved with P^5 space discretizations. Again, the time-step size used for the time convergence test is limited by accuracy requirements and not by CFL stability. Demonstration of time convergence of the fourth-order implicit scheme of Eq. (16) with P^5 polynomial expansions is very costly. Convergence tests with P^5 polynomials require meshes that have $\Delta x \approx 0.01$ (e.g., CFL = 10), to have at least one order of magnitude difference for $\Delta t \approx 0.1$, which is imposed by time-accuracy requirements. Stability of implicit time integration was again maintained in two dimensions for CFL as large as 10,000.

In Fig. 9, the computational cost of the explicit TVD-RK3 and RK4 methods and the cost of the second- and fourth-order-accurate implicit methods is compared. It is evident that time-accurate advancement of the numerical solution with implicit methods is advantageous in two dimensions, in which an order of magnitude reduction in computing time could be achieved even for very low tolerance of time-integration error. This trend certainly carries over to three dimensions, in which even larger savings in computational time could be expected.

Implicit time marching is applied next for the numerical solution of more complex aeroacoustic problems, which are of interest to practical applications. For these applications, the small size of elements required for accurate geometry representation could impose severe stability limitations for explicit time-marching methods with high-order DG spacial discretizations. Scattering due to a pressure pulse $\exp[A(x_o^2 + y_o^2)/w]$, which is used as an initial condition for the numerical solution of the governing equations from the surface of a cylinder, is computed using implicit time marching. For comparison, solutions were computed with explicit schemes. For accurate representation of the cylinder, 45 elements are used on its surface. The smallest element size is $h = 0.07 = \pi/45$, and the theoretical stability limit of the RK3 method [7] is $\Delta t/h \leq 0.13$. However, in practice, due to the presence of computational boundaries, we were not able to obtain stable solutions with time steps larger than $\Delta t = 0.0001$ or CFL ≤ 0.0035. The CFL restriction of the fourth-order-accurate (in space) DG method appears much more restrictive than a fourth-order finite difference method, which, for the same problem, was found to be stable for CFL ≤ 0.5. It should be noted that equally accurate solutions could have been obtained with the DG method if fewer elements with curved boundaries were used to represent the cylinder [34]. However, for realistic three-dimensional configurations such as wings and other aerodynamic bodies, the use of elements with a complex boundary shape is not straightforward.

The computed acoustic pressure field at time $T = 10$ for scattering of the pulse $\exp[\log 2(x_o^2 + y_o^2)/0.04]$, located at $R_o = 4$ from the

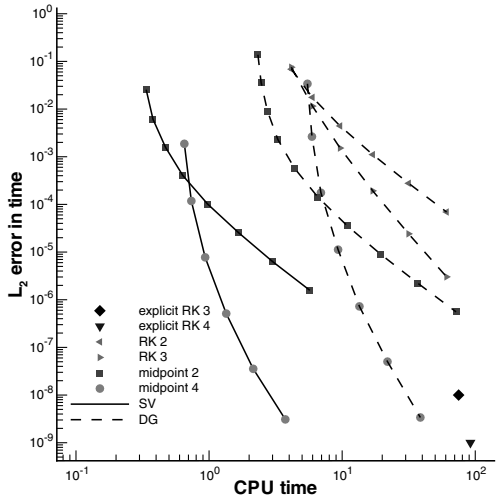

Fig. 7 Computational cost of implicit schemes.

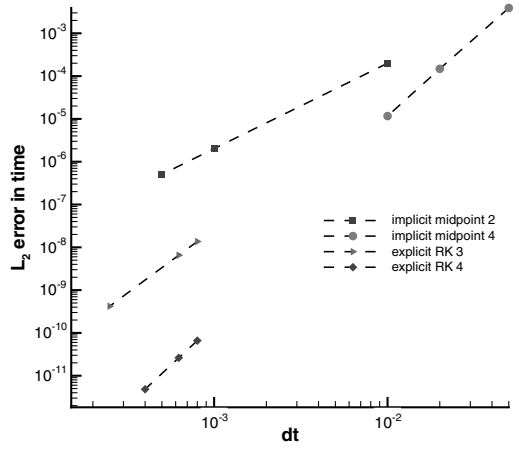

Fig. 8 Time convergence in two dimensions.

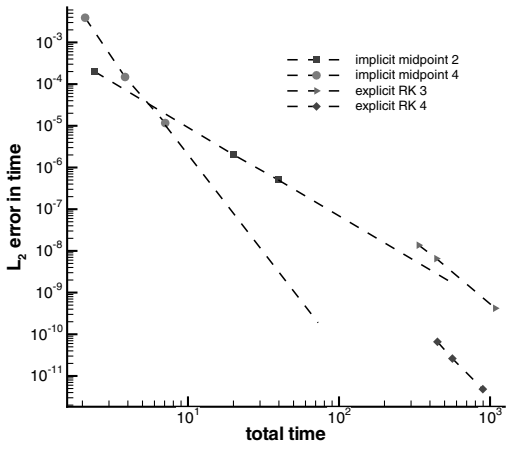

Fig. 9 Computational cost in two dimensions.

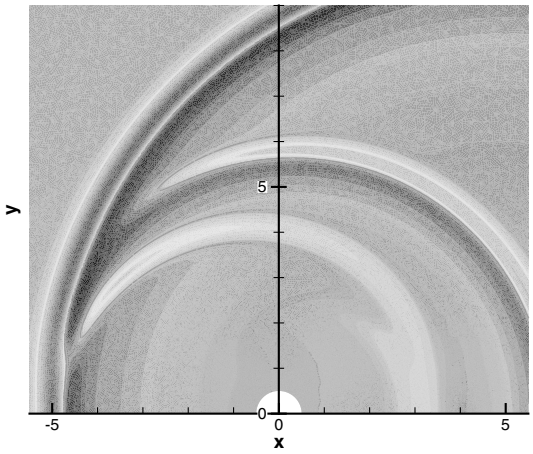

Fig. 10 Computed acoustic pressure field for scattering of a pulse from the surface of a cylinder.

surface of a cylinder of radius $R = 0.5$, is shown in Fig. 10. Comparisons of the computed pressure with the exact result [33] are shown in Figs. 11 and 12. Figures 11a and 11b show comparisons of the computed and exact pressure for time $t = 5$–10 for the points $R = 5$, $\theta = 90$ deg and $R = 5$, $\theta = 135$ deg, respectively. Figures 12a and 12b show comparisons of the computed and exact pressure for points located at $0.5 \leq r \leq 10$ for time $t = 4$, $\theta = 45$ deg and time $t = 7$, $\theta = 90$ deg. The comparisons of Figs. 11 and 12 with the exact result clearly demonstrate the ability of high-order-accurate time-marching methods to perform accurate time

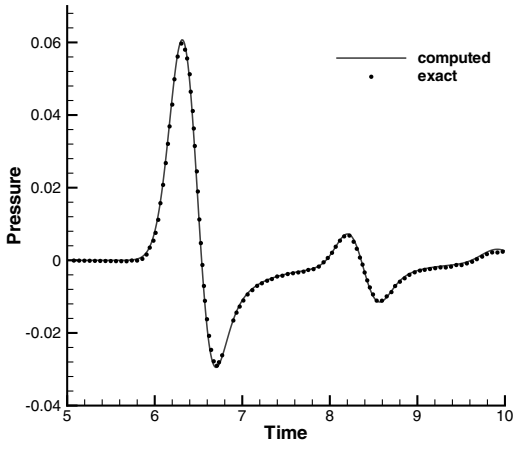

a) $\theta = 90$ deg, $r = 5$

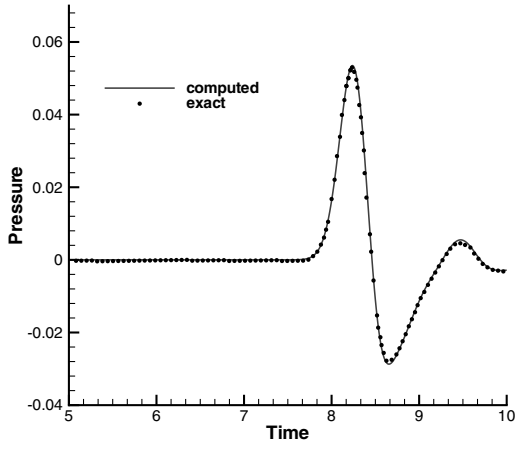

b) $\theta = 135$ deg, $r = 5$

Fig. 11 Comparison of the computed and the exact solution for time $5 \leq t \leq 10$.

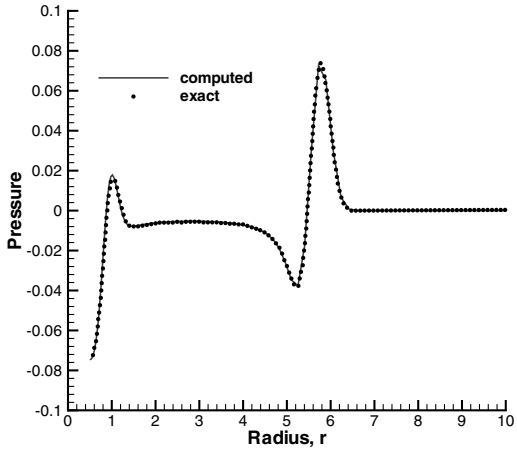

a) $\theta = 45$ deg, $t = 4$

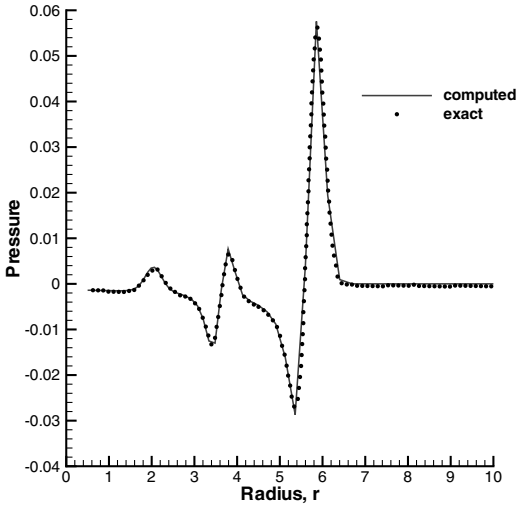

b) $\theta = 90$ deg, $t = 7$

Fig. 12 Comparison of the computed and the exact solution for two azimuthal locations.

advancement with reasonably high time steps. These computations were obtained with the fourth-order-accurate method of Eq. (16) and a time step $\Delta t = 0.01$ to ensure sufficient accuracy in time. It was found, however, that quite accurate solutions could be obtained even with time step $\Delta t = 0.1$. For the RK3 [6], the allowable time step was $\Delta t \approx 0.0001$. This reduction in time step by two orders of magnitude makes the computational cost with the explicit schemes in domains with small cells quite large.

For the computation obtained with $\Delta t = 0.01$, the computing cost of the implicit scheme was 30 times smaller than the cost of the explicit scheme. On the other hand, the error of the explicit scheme with respect to the exact solution was still acceptable and lower than 1%, which is comparable to the error obtained by the explicit time-integration methods. Analogous reduction in computing time was achieved for the numerical solution obtained with $\Delta t = 0.1$ and the error was approximately 2%. It appears, therefore, that for accurate aeroacoustic computations in two- and three-dimensional complex geometries, implicit high-order schemes can offer some benefit.

VI. Conclusions

Implicit high-order-accurate time-marching methods were applied for SV and DG space discretizations of linear conservation laws. It was demonstrated that the use of implicit methods for practical aeroacoustic computations with SV or DG discretizations is advantageous despite the computational time that is required for the solution of the large linear system. Comparisons of computed solutions obtained for problems with exact solutions demonstrated

that higher-order implicit methods outperform explicit and lower-order implicit methods for computational aeroacoustics with stringent accuracy requirements. In addition, implicit time-marching methods make practical the use of high-order spatial discretizations for complex domain aeroacoustic problems in which presence of small size elements is inevitable.

Acknowledgment

This effort was sponsored by the U.S. Air Force Office of Scientific Research, U.S. Air Force Materiel Command under grant FA8655-03-1-3085 and under grant GRID-APP of the General Secretariat for Research and Technology, Greece.

References

[1] Cockburn, B., and Shu, C. W. "The Runge-Kutta Discontinuous Galerkin Method for Conservation Laws, 5: Multidimensional Systems," *Journal of Computational Physics*, Vol. 141, No. 2, 1998, pp. 199–224.

[2] Wang, Z. J., "Spectral (Finite) Volume Method for Conservation Laws on Unstructured Grids. Basic Formulation: Basic Formulation," *Journal of Computational Physics*, Vol. 178, No. 1, 2002, pp. 210–251.

[3] Wang, Z. J., and Liu, Y., "Spectral (Finite) Volume Method for Conservation Laws on Unstructured Grids 2: Extension to Two-Dimensional Scalar Equation," *Journal of Computational Physics*, Vol. 179, No. 2, 2002, pp. 665–697.

[4] Wang, Z. J., Zhang, L., and Liu, Y., "Spectral (Finite) Volume Method for Conservation Laws on Unstructured Grids, 4: Extension to Two-Dimensional Systems," *Journal of Computational Physics*, Vol. 194, No. 2, 2004, pp. 716–741.

[5] Liu, Y., Vinokur, M., and Wang, Z. J., "Spectral (Finite) Volume Method for Conservation Laws on Unstructured Grids, 5: Extension to Three-Dimensional Systems," *Journal of Computational Physics*, Vol. 212, No. 2, 2006, pp. 454–472.

[6] Toulopoulos, I., and Ekaterinaris, J. A., "High-Order Discontinuous-Galerkin Discretizations for Computational Aeroacoustics in Complex Domains," *AIAA Journal*, Vol. 44, No. 3, 2006, pp. 502–511; also AIAA Paper 2004-0522.

[7] Atkins, H., and Shu, C. W., "Quadrature-Free Implementation of the Discontinuous Galerkin Method for Hyperbolic Equations," *AIAA Journal*, Vol. 36, Nos. 5–6, 1998, pp. 775–782.

[8] Ekaterinaris, J. A., "Performance of High-Order Accurate Low-Diffusion Numerical Schemes for Compressible Flow," *AIAA Journal*, Vol. 42, No. 3, 2004, pp. 493–500.

[9] Ekaterinaris, J. A., "High-Order Accurate, Low Numerical Diffusion Methods for Aerodynamics," *Progress in Aerospace Sciences*, Vol. 41, Nos. 3–4, 2005, pp. 192–300.

[10] Rasetarinera, P., and Hussaini, M. Y., "An Efficient Implicit Discontinuous Galerkin Method," *Journal of Computational Physics*, Vol. 172, No. 2, 2001, pp. 718–738.

[11] Bassi, F., Crivellini, A., Rebay, S., and Savini, M., "Discontinuous Galerkin Solutions of the Reynolds-Averaged Navier–Stokes and K-ω Turbulence Model Equations," *Computers and Fluids*, Vol. 34, Nos. 4–5, 2004, pp. 507–540.

[12] Wang, L., and Mavriplis, D., "Implicit Solution of the Unsteady Euler Equations for High-Order Accurate Discontinuous Galerkin Discretizations," AIAA Paper 2006-0109, Jan. 2006.

[13] Persson, P. O., and Peraire, J., "An Efficient Low Memory Implicit DG Algorithm for Time Dependent Problems," AIAA Paper 2006-0113, Jan. 2006.

[14] Fidkowski, K. J., Oliver, T. A., Lu, J., and Darmofal, D. L., "p-Multigrid Solution of High-Order Discontinuous Galerkin Discretizations of the Compressible Navier–Stokes Equations," *Journal of Computational Physics*, Vol. 207, No. 1, 2005, pp. 92–113.

[15] Helenbrook, B., Mavriplis, D., and Atkins, H., "Analysis of p-multigrid for Continuous and Discontinuous Finite Element Discretizations," AIAA Paper 2003-3989.

[16] Nastase, C. R., and Mavriplis, D. J., "High-Order Discontinuous Galerkin Methods Using Spectral Multigrid Approach," AIAA Paper 2005-1268, Jan. 2005.

[17] Nastase, C. R., and Mavriplis, D. J., "Discontinuous Galerkin Methods Using an hp-Multigrid Solver for Inviscid Compressible Flows on Three-Dimensional Unstructured Meshes," AIAA Paper 2006-0107, Jan. 2006.

[18] Titarev, V. A., and Toro, E. F., "ADER Schemes for Scalar Non-Linear Hyperbolic Conservation Laws with Source Terms in Three-Space Dimensions," *Journal of Computational Physics*, Vol. 202, No. 1, 2005, pp. 196–215.

[19] Titarev, V. A., and Toro, E. F., "ADER Schemes for Three-Dimensional Non-Linear Hyperbolic Systems," *Journal of Computational Physics*, Vol. 204, No. 2, 2005, pp. 715–736.

[20] Van der Vegt, J. J. W., and van der Ven, H., "Space–Time Discontinuous Galerkin Finite Element Method with Dynamic Grid Motion for Inviscid Compressible Flows, 1: General Formulation," *Journal of Computational Physics*, Vol. 182, No. 2, 2002, pp. 546–585.

[21] Klaij, C. M., van der Vegt, J. J. W., and van der Ven, H., "Space–Time Discontinuous Galerkin Method for the Compressible Navier–Stokes Equations," *Journal of Computational Physics*, Vol. 217, No. 2, 2006, pp. 589–611.

[22] Lin, R. K., and Sheu, W. H., "A Four-Step Time Splitting Scheme for Convection-Diffusion Equation," *Numerical Heat Transfer, Part B, Fundamentals*, Vol. 45, No. 3, 2004, pp. 263–281.

[23] Lin, R. K., and Sheu, T. W. H., "Application of Dispersion-Relation-Preserving Theory to Develop a Two-Dimensional Convection Diffusion Scheme," *Journal of Computational Physics*, Vol. 208, No. 2, 2005, pp. 493–526.

[24] De Frutos, J., and Sanz-Serna, J. M., "An Easy Implementable Fourth-Order Method for Time Integration of Wave Problems," *Journal of Computational Physics*, Vol. 160, No. 1, 1992, pp. 160–168.

[25] Isono, S., and Zingg, D. W., "A Runge-Kutta-Newton-Krylov Algorithm for Fourth-Order Implicit Time Marching Applied to Unsteady Flows," AIAA Paper 2004-0433, Jan. 2004.

[26] Bijl, H., Carpenter, M. H., Vatsa, V. N., and Kennedy, C. A., "Implicit Time Integration Schemes for Unsteady Compressible Navier–Stokes Equations: Laminar Flow," *Journal of Computational Physics*, Vol. 179, No. 1, 2002, pp. 313–329.

[27] Zhang L. P., and Wang, Z. J., "A Block LU-SGS Implicit Dual Time-Stepping Algorithm for Hybrid Dynamic Meshes," *Computers and Fluids*, Vol. 33, No. 7, 2004, pp. 891–916.

[28] Ainsworth, M., "Dispersive and Dissipative Behaviour of High Order Discontinuous Galerkin Finite Element Methods," *Journal of Computational Physics*, Vol. 198, No. 1, 2004, pp. 106–130.

[29] Hu, F. Q., Hussaini, M. Y., and Manthey, J. L., "Low-Dissipation and Low-Dispersion Runge–Kutta Schemes for Computational Acoustics," *Journal of Computational Physics*, Vol. 124, No. 1, 1996, pp. 177–191.

[30] Zhang, M., and Shu, C. W., "An Analysis of and a Comparison Between the Discontinuous Galerkin and the Spectral Finite Volume Methods," *Computers and Fluids*, Vol. 34, Nos. 4–5, 2005, pp. 581–592.

[31] Saad, Y., *Iterative Methods for Sparse Linear Systems*, 2nd ed., Society for Industrial and Applied Mathematics, Philadelphia, Jan. 2000.

[32] Hardin, J. C., Ristorcelli, J. R., and Tam, C. K., "ICASE/LaRC Workshop on Benchmark Problems in Computational Aeroacoustics (CAA)," NASA CP 3300, 1995.

[33] Tam, C. K. W., and Hardin, J. C., "Second Computational Aeroacoustics (CAA) Workshop on Benchmark Problems," NASA CP 3352, Nov. 1997.

[34] Bassi, F., and Rebay, S., "High-Order Accurate Discontinuous Finite Element Solution of the 2D Euler Equations," *Journal of Computational Physics*, Vol. 138, No. 2, 1997, pp. 251–285.

K. Powell
Associate Editor